3-D Numerical Mode-Matching (NMM) Method for Resistivity Well-Logging Tools

Guo-Xin Fan, *Senior Member, IEEE*, Qing Huo Liu, *Senior Member, IEEE*, and Sean P. Blanchard

***Abstract*—A three-dimensional (3-D) numerical mode-matching (NMM) method is presented for Poisson's equation in general inhomogeneous media. It reduces the original 3-D problem into a series of two-dimensional (2-D) eigenvalue problems plus a one-dimensional (1-D) layered medium problem, which can be modeled efficiently by a recursion procedure. The algorithm is tested for several 3-D inhomogeneous media and an excellent agreement between the NMM and analytical solutions is obtained for all test cases. We demonstrate some typical applications of the 3-D NMM algorithm in resistivity well logging, including invasion zones of noncircular shape, vertical and horizontal fractures, and horizontal wells. The solution procedure proposed is directly applicable to wave propagation in 3-D inhomogeneous media.**

***Index Terms*—Inhomogeneous media, layered media, numerical mode-matching (NMM) method, resistivity well logging.**

I. Introduction

LOW-FREQUENCY electrode-type resistivity tools are widely used to probe the resistivity distribution of formation in electrical well logging [1], [2]. These electrode-type resistivity tools usually operate at very low frequency (below a few kilohertz), while the measurement region interested is limited to a relatively small region (a few meters) around the electrodes in the borehole. Therefore, the frequency effects can be ignored, and the electrostatic or dc approximation is adequate for the modeling of these resistivity tools.

Various numerical methods have been used to model the resistivity tools, such as analytical methods [3]–[5], integral equation method [6], finite-element method (FEM) [7], [8], and numerical mode-matching (NMM) method [9]–[15]. Among these methods, the FEM is a most general-purpose numerical method, while the NMM method has been shown to be more efficient than a direct use of the FEM for the well-logging problems. The efficiency of the NMM method is based on the idea that a higher dimensional problem can be reduced to a series of lower dimensional problems. For example, a two-dimensional (2-D) problem is reduced to one-dimensional (1-D) problems, and the field in all layers is obtained in a recursive scheme.

The NMM method as an efficient algorithm has been used to model various multiregion vertically and cylindrically stratified inhomogeneous media for both high- and low-frequency applications [9]–[21]. However, so far the applications of the NMM method have been limited to 2-D and two-and-a-half-dimensional (2.5-D) problems. Although 2-D inhomogeneous models, such as axisymmetric media, have found many successful applications in realistic well-logging, the media in general are three-dimensional (3-D) inhomogeneous. Therefore, it is necessary to develop a 3-D algorithm for modeling Poisson's equation in resistivity well logging.

In this work, we extend for the first time the NMM method to 3-D inhomogeneous media and apply it to model electric potential distribution in well logging. Although this work treats the electric potential problems, the solution procedure presented here can be directly applied to wave problems.

II. Formulation

In general, a 3-D inhomogeneous medium can be regarded as a horizontally-layered multiregion medium as shown in Fig. 1. We break this 3-D inhomogeneous medium into N horizontal layers of arbitrary thickness. Each layer is modeled as being homogeneous in the vertical direction, but inhomogeneous in the horizontal plane, i.e., the conductivity σ_n of each layer is the function of only x and y. The interface between nth layer and $(n+1)$th layer is $z = z_n$, with $z_1 < z_2 < \cdots < z_{N-1}$. We also assume that $z_0 \to -\infty$ and $z_N \to \infty$. Then, using the characteristic function $C(z, z_{n-1}, z_n)$ (which is one for z in layer n, and zero otherwise), we can write the 3-D conductivity distribution as $\sigma(x, y, z) = \sum_n C(z, z_{n-1}, z_n)\sigma_n(\boldsymbol{\rho})$, where $\boldsymbol{\rho} = (x, y)$.

For such a horizontally layered conductive medium, the electric potential within each region satisfies Poisson's equation

$$\nabla_\tau \cdot \sigma_n(\boldsymbol{\rho})\nabla_\tau u(\boldsymbol{\rho}, z) + \sigma_n(\boldsymbol{\rho})\frac{\partial^2}{\partial z^2}u(\boldsymbol{\rho}, z) = -\nabla \cdot \mathbf{J}, \quad z_{n-1} < z < z_n, \qquad n = 1, \cdots, N \tag{1}$$

where $\mathbf{J}$ is the external electric current density. We aim to solve this equation to compute the electric potential distribution in all regions.

This partial differential equation can be solved by the 3-D finite-element method (FEM). However, as shown for 2-D and 2.5-D problems [9]–[21], the NMM method is far more efficient, especially for layered media with large layer thicknesses. Here, in the 3-D NMM method, we first solve N 2-D eigenvalue

Manuscript received August 26, 1999; revised August 2, 2000. This work was supported by the U.S. EPA through PECASE Grant CR-825-225-010 and by the NSF through CAREER Grant ECS-9702195.

G.-X. Fan was with Klipsch School of Electrical and Computer Engineering, New Mexico State University, Las Cruces, NM 88003 USA. He is now with the Department of Electrical and Computer Engineering, Duke University, Durham, NC 27708-0291 USA (e-mail: gfan@ee.duke.edu).

Q. H. Liu is with the Department of Electrical and Computer Engineering, Duke University, Durham, NC 27708-0291 USA (qhliu@ee.duke.edu).

S. P. Blanchard was with Klipsch School of Electrical and Computer Engineering, New Mexico State University, Las Cruces, NM 88003 USA. He is now with Silicon Graphics Inc., Los Alamos National Lab, Los Alamos, NM 87544 USA.

Publisher Item Identifier S 0018-926X(00)09831-8.

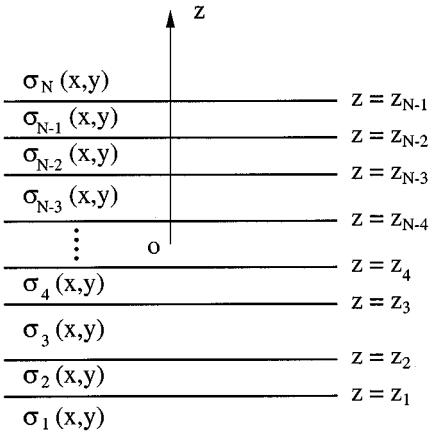

Fig. 1. An N-layer inhomogeneous conductive medium.

problems for all layers. The mode conversion between adjacent layers is then accounted for by the local reflection and transmission matrices. Finally, the multiple reflections among all layers are modeled by a recursion scheme through global reflection matrices.

A. 2-D Eigenvalue Problems

We first consider an eigenvalue problem for layer ℓ. From (1), the 3-D eigenfunctions for the ℓth layer can be written as $\Phi_j(\boldsymbol{\rho})e^{-k_{jz}z}$, where the 2-D eigenvalue problem for the ℓth layer can be defined as

$$\nabla_\tau \cdot \sigma_\ell(\boldsymbol{\rho})\nabla_\tau\Phi_j(\boldsymbol{\rho}) + \sigma_\ell(\boldsymbol{\rho})k_{jz}^2\Phi_j(\boldsymbol{\rho}) = 0 \qquad (2)$$

with Dirichlet $(\Phi_j = 0)$ or Neumann $(\partial\Phi_j/\partial n = 0)$ boundary conditions at the outer boundary $\boldsymbol{\rho} \in \partial S$. It can be shown that the squared modal attenuation constants k_{jz}^2 are real and nonnegative.

For an inhomogeneous medium with an arbitrary boundary ∂S, the above eigenvalue problem does not have an analytical solution. In this work, we use a 2-D FEM with triangular cells to solve the 2-D eigenvalue equation (2) with an appropriate boundary condition on ∂S. The eigenfunctions are expanded in terms of basis functions and the resulting generalized matrix eigenvalue equation is of the form

$$\overline{\mathbf{A}} \cdot \mathbf{v}_j = k_{jz}^2\, \overline{\mathbf{B}} \cdot \mathbf{v}_j \qquad (3)$$

where

$\overline{\mathbf{A}}, \overline{\mathbf{B}}$ $L \times L$ sparse banded symmetric matrices (L is the number of FEM nodal points);
k_{jz}^2 eigenvalue;
$\mathbf{v}_j$ corresponding eigenvector of length L.

In the FEM implementation, the matrices $\overline{\mathbf{A}}$ and $\overline{\mathbf{B}}$ are assembled from the elemental $\overline{\mathbf{A}}^e$ and $\overline{\mathbf{B}}^e$, respectively, incorporating the boundary conditions. For linear triangle elements, the entries of $\overline{\mathbf{A}}^e$ and $\overline{\mathbf{B}}^e$ are given by

$$A_{ij}^e = \iint_{\Omega^e} \sigma_\ell^e \left(\frac{\partial N_i^e}{\partial x}\frac{\partial N_j^e}{\partial x} + \frac{\partial N_i^e}{\partial y}\frac{\partial N_j^e}{\partial y} \right) dx\, dy \qquad (4)$$

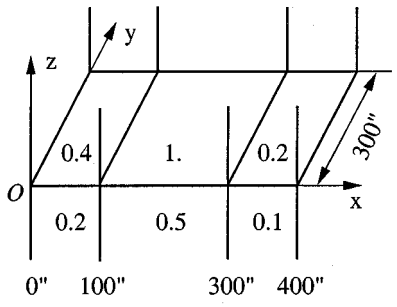

(a)

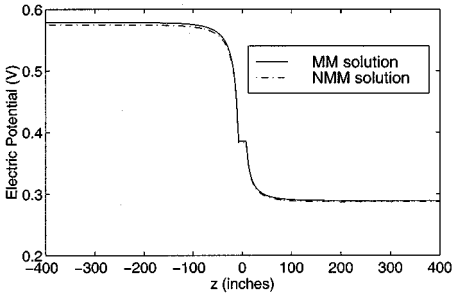

(b)

Fig. 2. Comparison of the NMM result with MM result for a two-layer three-block medium. (a) Geometry—the conductivity value shown is in siemens per meter for this and all following figures. (b) Electric potential distribution—the point charge source and receiver are moving along the z direction, with $x = x' = 300$ in, $y = y' = 150$ in, and $|z - z'| = 16$ in.

$$B_{ij}^e = \iint_{\Omega^e} \sigma_\ell^e N_i^e N_j^e\, dx\, dy \qquad i, j = 1, 2, 3 \qquad (5)$$

where

Ω^e domain of the eth element;
σ_ℓ^e conductivity of the eth element in the ℓth layer;
N_i^e expansion function.

The details of the above formulation can be found in general FEM books, e.g., [22]. In addition, higher order elements may be chosen to further improve the accuracy of solution and reduce the number of nodes, hence, the size of matrices $\overline{\mathbf{A}}$ and $\overline{\mathbf{B}}$.

Equation (3) can be solved by several special purpose eigensolvers available. In practical NMM computation, only the first M eigenvalues and associated eigenmodes are necessary to give a convergent field solution.

From (2), we can show that the above eigenfunctions have the following orthogonality:

$$\langle \Phi_i,\, \sigma_\ell \Phi_j \rangle = \int_S \Phi_i(\boldsymbol{\rho})\sigma_\ell(\boldsymbol{\rho})\Phi_j(\boldsymbol{\rho})\, dS = \delta_{ij} \qquad (6)$$

where δ_{ij} is the usual Kronecker delta function. It can be readily shown that the above orthogonality has an equivalent form associated with (3) as

$$\mathbf{v}_i^t \cdot \overline{\mathbf{B}} \cdot \mathbf{v}_j = \delta_{ij} \qquad (7)$$

where superscript t denotes the transpose of a vector or matrix. The eigenfunctions form a complete set and a similar derivation can be found in [16]. Therefore, the field within the layer can

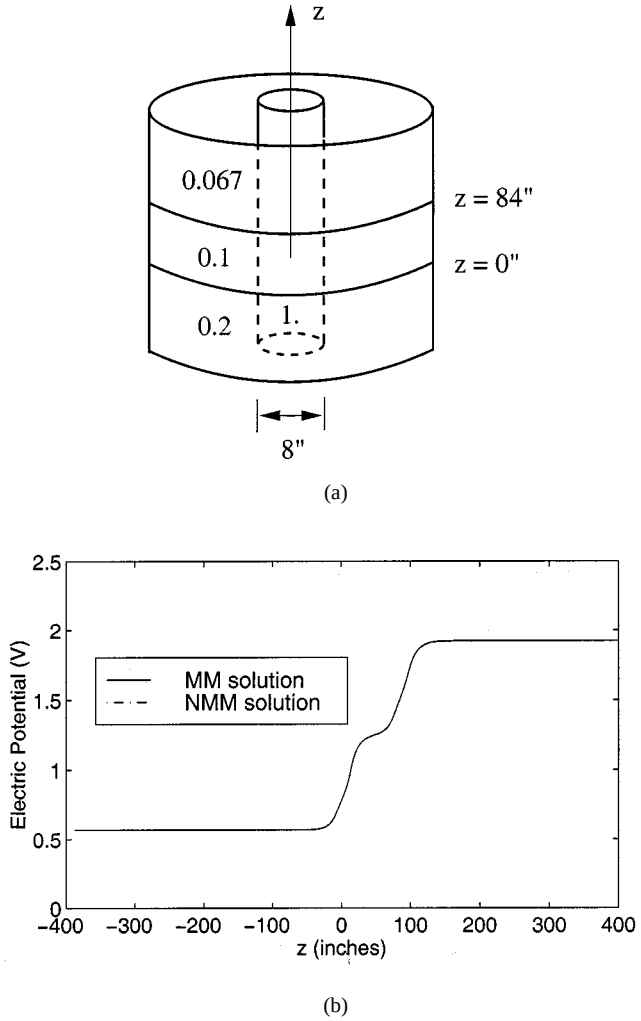

Fig. 3. Comparison of the NMM result with MM result for a three-layer coaxial cylinder medium. (a) Geometry. (b) Electric potential distribution. The point charge source and receive are moving along the z direction, with $x = x' = 0$, $y = -y' = 0.1$ in, and $|z - z'| = 16$ in.

be expanded in terms of these eigenmodes and the expansion coefficients are determined uniquely.

The Green's function of (1), with $\nabla \cdot \mathbf{J} = \delta(\mathbf{r} - \mathbf{r}')$ in the absence of all horizontal boundaries, can be expanded in terms of the above eigenfunctions as

$$G(\mathbf{r}, \mathbf{r}') = \sum_j \frac{1}{2k_{jz}} \Phi_j(\boldsymbol{\rho}') \Phi_j(\boldsymbol{\rho}) e^{-k_{jz}|z-z'|}. \tag{8}$$

Using vector notation [16], (8) can be written in a more concise form

$$G(\mathbf{r}, \mathbf{r}') = \boldsymbol{\Phi}^t(\boldsymbol{\rho}) \cdot e^{-\overline{\mathbf{K}}_z|z-z'|} \cdot \mathbf{S}(\boldsymbol{\rho}') \tag{9}$$

where

- $\boldsymbol{\Phi}^t(\boldsymbol{\rho})$ column vector of length M containing the eigenfunction $\Phi_j(\boldsymbol{\rho})$;
- $\overline{\mathbf{K}}_z$ $M \times M$ diagonal matrix containing k_{jz};
- $\mathbf{S}(\boldsymbol{\rho}')$ excitation coefficient vector of length M containing the remaining terms in (8).

B. A Half-Space Problem

The solution in (9) gives the potential distribution for an infinitely thick layer ℓ (i.e., $z_{\ell-1} \to -\infty$ and $z_\ell \to \infty$). Now when two semi-infinitely thick layers, say layers m and $m+1$, form a half-space with an interface at $z = z_m$, mode conversion occurs at the interface in order to satisfy the boundary conditions. In the NMM method, this mode conversion is described by the local reflection and transmission matrices. Assuming a source in region m, the fields in the two regions are given by

$$G_m(\mathbf{r}, \mathbf{r}') = \boldsymbol{\Phi}_m^t(\boldsymbol{\rho}) \cdot \left[e^{-\overline{\mathbf{K}}_{mz}|z-z'|} + e^{-\overline{\mathbf{K}}_{mz}(z_m - z)} \cdot \overline{\mathbf{R}}_{m,m+1} \cdot e^{-\overline{\mathbf{K}}_{mz}(z_m - z')} \right] \cdot \mathbf{S}_m(\boldsymbol{\rho}') \tag{10}$$

$$G_{m+1}(\mathbf{r}, \mathbf{r}') = \boldsymbol{\Phi}_{m+1}^t(\boldsymbol{\rho}) \cdot e^{-\overline{\mathbf{K}}_{m+1,z}(z - z_m)} \cdot \overline{\mathbf{T}}_{m,m+1} \cdot e^{-\overline{\mathbf{K}}_{mz}(z_m - z')} \cdot \mathbf{S}_m(\boldsymbol{\rho}') \tag{11}$$

where $\overline{\mathbf{R}}_{m,m+1}$ and $\overline{\mathbf{T}}_{m,m+1}$ are the local reflection and transmission matrices of dimension $M \times M$. Using the continuity conditions for electric potentials and the normal electric currents at $z = z_m$, i.e.,

$$\left. G_m \right|_{z=z_m} = \left. G_{m+1} \right|_{z=z_m}$$
$$\sigma_m \left. \frac{\partial G_m}{\partial z} \right|_{z=z_m} = \sigma_{m+1} \left. \frac{\partial G_{m+1}}{\partial z} \right|_{z=z_m} \tag{12}$$

and applying the orthogonality relation of the eigenfunctions, we obtain

$$\overline{\mathbf{T}}_{m,m+1} = \left(\overline{\mathbf{K}}_{m+1,z} + \overline{\mathbf{Q}}_{m,m+1}^t \cdot \overline{\mathbf{K}}_{m,z} \cdot \overline{\mathbf{Q}}_{m,m+1} \right)^{-1} \cdot \overline{\mathbf{Q}}_{m,m+1}^t \cdot \overline{\mathbf{K}}_{m,z} \tag{13}$$

$$\overline{\mathbf{R}}_{m,m+1} = \overline{\mathbf{Q}}_{m,m+1} \cdot \overline{\mathbf{T}}_{m,m+1} - \overline{\mathbf{I}} \tag{14}$$

where $\overline{\mathbf{I}}$ is an identity matrix, and $\overline{\mathbf{Q}}_{m,m+1}$ is the mode conversion matrix between mth and $(m+1)$th layers

$$\overline{\mathbf{Q}}_{m,m+1} = \langle \boldsymbol{\Phi}_m, \sigma_m \boldsymbol{\Phi}_{m+1}^t \rangle. \tag{15}$$

Note the conversion of modes from layer m to layer $m+1$ are completely described by the local reflection and transmission matrices $\overline{\mathbf{R}}_{m,m+1}$ and $\overline{\mathbf{T}}_{m,m+1}$. Similarly, when the source is located in layer $m+1$, we can derive the expressions for $\overline{\mathbf{R}}_{m+1,m}$ and $\overline{\mathbf{T}}_{m+1,m}$.

C. The Multilayer Problem—Mode-Matching Process

Now we turn to the multilayer medium in Fig. 1. Because of multiple interfaces, multiple reflections occur within the layers. The mode matching is a process to derive a recursive procedure to account for the multiple reflections through the global reflection matrices. The NMM solution procedure here is parallel to those in the 2-D and 2.5-D problems. We only provide the final formulas and more details can be found in [16], [17], and [20].

For an N-region problem, if the source is embedded in region m, the expression of Green's function in region n ($n = m$, $n > m$ and $n < m$) can be constructed as

$$G_m(\mathbf{r}, \mathbf{r}') = \boldsymbol{\Phi}_m^t(\boldsymbol{\rho}) \cdot \Big[e^{-\overline{\mathbf{K}}_{mz}|z-z'|} \cdot \mathbf{S}_m(\boldsymbol{\rho}') + e^{-\overline{\mathbf{K}}_{mz}(z-z_{m-1})} \cdot \mathbf{C}_m + e^{-\overline{\mathbf{K}}_{mz}(z_m-z)} \cdot \mathbf{D}_m \Big] \tag{16}$$

$$G_n(\mathbf{r}, \mathbf{r}') = \boldsymbol{\Phi}_n^t(\boldsymbol{\rho}) \cdot \Big[e^{-\overline{\mathbf{K}}_{nz}(z-z_n)} + e^{\overline{\mathbf{K}}_{nz}(z-z_n)} \cdot \tilde{\overline{\mathbf{R}}}_{n,n+1} \Big] \cdot \mathbf{A}_n \qquad n > m \tag{17}$$

$$G_n(\mathbf{r}, \mathbf{r}') = \boldsymbol{\Phi}_n^t(\boldsymbol{\rho}) \cdot \Big[e^{-\overline{\mathbf{K}}_{nz}(z-z_{n-1})} \cdot \tilde{\overline{\mathbf{R}}}_{n,n-1} + e^{\overline{\mathbf{K}}_{nz}(z-z_{n-1})} \Big] \cdot \mathbf{B}_n \qquad n < m \tag{18}$$

where $\mathbf{A}_n$, $\mathbf{B}_n$, $\mathbf{C}_m$ and $\mathbf{D}_m$ are the expansion coefficient vectors to be determined and $\tilde{\overline{\mathbf{R}}}_{n,n\pm1}$ are the global reflection matrices.

Applying the constraint conditions [16], [17] to these regions, we obtain the recursive relations for the matrices $\tilde{\overline{\mathbf{R}}}_{n-1,n}$ and $\tilde{\overline{\mathbf{R}}}_{n+1,n}$ as

$$\tilde{\overline{\mathbf{R}}}_{n\pm1,n} = \overline{\mathbf{R}}_{n\pm1,n} + \overline{\mathbf{T}}_{n,n\pm1} \cdot \overline{\mathbf{P}}_{n-1,n} \cdot \tilde{\overline{\mathbf{R}}}_{n,n\mp1} \cdot \overline{\mathbf{P}}_{n-1,n} \cdot \overline{\mathbf{M}}_n^{(\pm)} \cdot \overline{\mathbf{T}}_{n\pm1,n} \tag{19}$$

where the propagator $\overline{\mathbf{P}}_{n-1,n}$ and multiple reflection matrix $\overline{\mathbf{M}}_n^{(\pm)}$ are given by

$$\overline{\mathbf{P}}_{n-1,n} = e^{-\overline{\mathbf{K}}_{nz}(z_n-z_{n-1})} \tag{20}$$

$$\overline{\mathbf{M}}_n^{(\pm)} = \Big[\bar{\mathbf{I}} - \overline{\mathbf{R}}_{n,n\mp1} \cdot \overline{\mathbf{P}}_{n-1,n} \cdot \tilde{\overline{\mathbf{R}}}_{n,n\pm1} \cdot \overline{\mathbf{P}}_{n-1,n} \Big]^{-1}. \tag{21}$$

Since $\tilde{\overline{\mathbf{R}}}_{1,0} = 0$ and $\tilde{\overline{\mathbf{R}}}_{N,N+1} = 0$, all global reflection matrices $\tilde{\overline{\mathbf{R}}}_{n,n-1}$ and $\tilde{\overline{\mathbf{R}}}_{n,n+1}$ can be obtained recursively from $\tilde{\overline{\mathbf{R}}}_{1,0}$ and $\tilde{\overline{\mathbf{R}}}_{N,N+1}$, respectively.

Using a similar procedure as in [16], [17], and [20], the remaining expansion coefficients $\mathbf{A}_n$, $\mathbf{B}_n$, $\mathbf{C}_m$, and $\mathbf{D}_m$ can be derived as follows:

$$\mathbf{A}_n = \overline{\mathbf{P}}_{n,n-1} \cdot \overline{\mathbf{M}}_n^{(-)} \cdot \mathbf{A}_{n-1} \tag{22}$$

$$\mathbf{B}_n = \overline{\mathbf{P}}_{n,n-1} \cdot \overline{\mathbf{M}}_n^{(+)} \cdot \mathbf{B}_{n+1} \tag{23}$$

$$\mathbf{C}_m = \tilde{\overline{\mathbf{M}}}_m^{(-)} \cdot \tilde{\overline{\mathbf{R}}}_{m,m-1} \cdot \Big[e^{-\overline{\mathbf{K}}_{mz}(z'-z_{m-1})} + \overline{\mathbf{P}}_{m-1,m} \cdot \tilde{\overline{\mathbf{R}}}_{m,m+1} \cdot e^{-\overline{\mathbf{K}}_{mz}(z_m-z')} \Big] \cdot \mathbf{S}_m(\boldsymbol{\rho}') \tag{24}$$

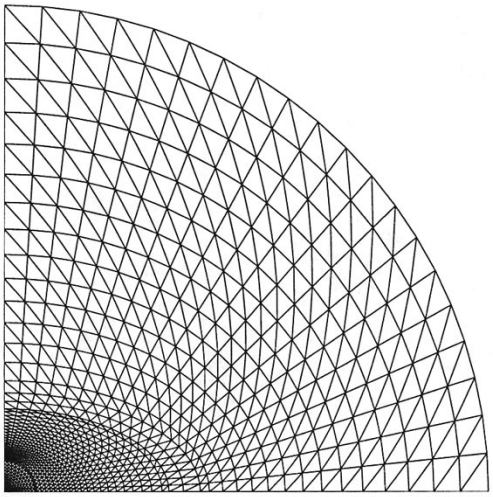

(a)

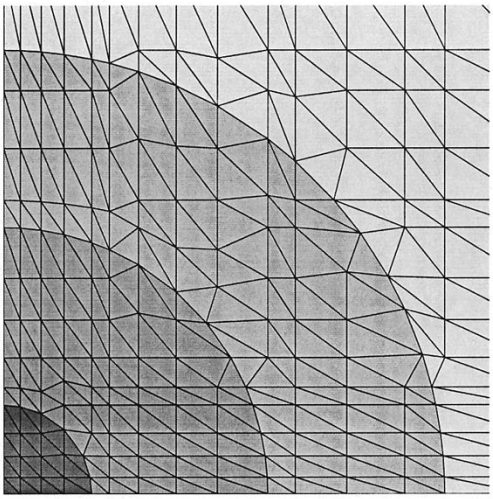

(b)

Fig. 4. Two typical grids for an elliptical borehole and invasion zone. (a) An elliptical grid. (b) A modified rectangular grid.

$$\mathbf{D}_m = \tilde{\overline{\mathbf{M}}}_m^{(+)} \cdot \tilde{\overline{\mathbf{R}}}_{m,m+1} \cdot \Big[\overline{\mathbf{P}}_{m-1,m} + \overline{\mathbf{P}}_{m-1,m} \cdot \tilde{\overline{\mathbf{R}}}_{m,m-1} \cdot e^{-\overline{\mathbf{K}}_{mz}(z'-z_{m-1})} \Big] \cdot \mathbf{S}_m(\boldsymbol{\rho}') \tag{25}$$

where

$$\tilde{\overline{\mathbf{M}}}_m^{(\pm)} = \Big[\bar{\mathbf{I}} - \tilde{\overline{\mathbf{R}}}_{m,m\mp1} \cdot \overline{\mathbf{P}}_{m-1,m} \cdot \tilde{\overline{\mathbf{R}}}_{m,m\mp1} \cdot \overline{\mathbf{P}}_{m-1,m} \Big]^{-1}. \tag{26}$$

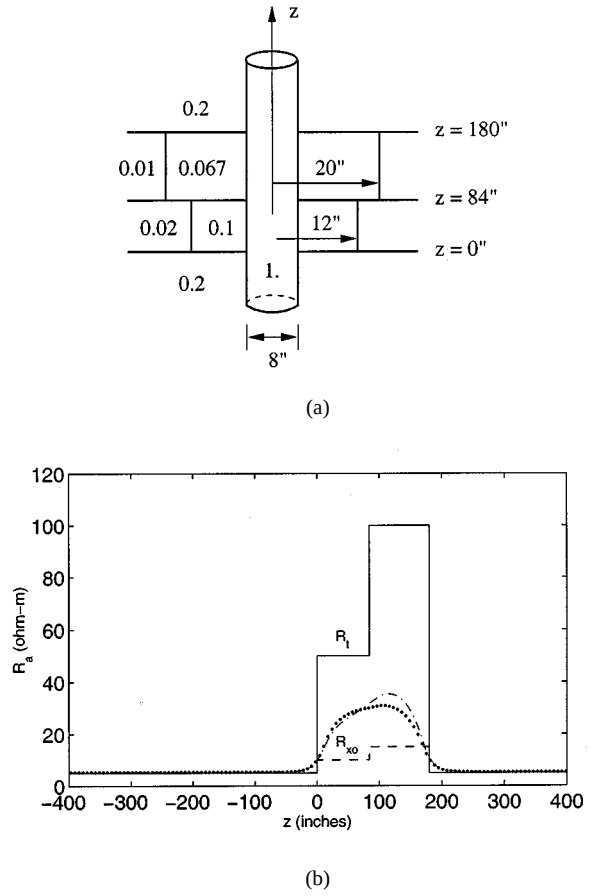

Fig. 5. Elliptical invasion and circular invasion. (a) Geometry. (b) Apparent resistivity distribution, $\cdots$ elliptical invasion, —— circular invasion. The straight lines indicate the formation true resistivity (R_t) and invasion resistivity (R_{x0}).

From (16)–(18), we can obtain the connecting conditions in the source region as

$$\mathbf{A}_m = e^{-\overline{\mathbf{K}}_{mz}(z_m - z')} \cdot \mathbf{S}_m(\boldsymbol{\rho}') + \overline{\mathbf{P}}_{m-1,m} \cdot \mathbf{C}_m \tag{27}$$

$$\mathbf{B}_m = e^{-\overline{\mathbf{K}}_{mz}(z' - z_{m-1})} \cdot \mathbf{S}_m(\boldsymbol{\rho}') + \overline{\mathbf{P}}_{m-1,m} \cdot \mathbf{D}_m. \tag{28}$$

With the above global reflection matrices and source excitation coefficient vectors, the field in all layers is, therefore, obtained through (16)–(18). Note that these matrices and vectors need to be solved only once. For any new source locations, the remaining computational efforts involve only matrix–vector multiplies, which are much faster than the solution of global reflection matrices.

Finally, we briefly discuss the computational cost in the 3-D NMM method. The 2-D eigenvalue problems require $O(NL^{\alpha}M)$ arithmetic operations in iterative solvers, where $\alpha = 2$ if full matrices are used, and $\alpha = 1.5$ if sparse matrices are used. More advanced methods may yield better results. In comparison, the mode matching process requires $O(NM^3)$ arithmetic operations, usually much cheaper than the eigenvalue problems since L is much larger than M. Therefore, the total computational cost is $O[N(C_1L^{\alpha}M + C_2M^3)]$ (C_1 and C_2 are constants) and can be dominated by the time spent in the eigensolvers. This is in contrast to the 2-D NMM method where L is about the same as M. As a result, reducing the computational complexity of the eigenvalue problems in 3-D NMM method becomes a more important issue than in 2-D NMM method. Currently, there are on-going efforts to improve the efficiency of eigensolvers [23], [24].

III. Numerical Results

In this section, we first test the 3-D NMM algorithm by comparing with the analytical mode-matching (MM) results and then illustrate its applications in resistivity well logging. In all examples, the dc source at $z - d/2$ and the observation point at $z + d/2$ move together in the z direction. The source-receiver spacing is $d = 16$ in and the borehole radius is 4 in.

As a test example, we consider a two-layer conductive medium as shown in Fig. 2(a). Each layer has three blocks, each having a constant conductivity. The Dirichlet boundary condition is applied to the outer boundaries at $x = 0, 400$ in and $y = 0, 300$ in. Fig. 2(b) shows the electric potential distribution due to a point charge moving along the z direction. Good agreement is observed between the NMM results and MM solutions.

Fig. 3(a) shows a three-layer coaxial cylinder, with an outer boundary radius of 1.5 m. To investigate the accuracy of the NMM solution, we developed an independent MM solution (see Appendix). In Fig. 3(b), we compare the results of the two solutions. Again excellent agreement is obtained between these solutions.

To illustrate the applications of 3-D NMM method, we consider several examples in resistivity well logging. The media in all cases are 3-D inhomogeneous and cannot be modeled by the previous 2-D and 2.5-D NMM algorithms. In these examples, we show the results for the apparent resistivity R_a defined as

$$R_a = 4\pi r u \tag{29}$$

where u is the electric potential produced by a unit point source and r is the distance between the source point and field point. In the following calculations, we take $\boldsymbol{\rho} = \boldsymbol{\rho}'$, hence, $r = d$.

For the well-logging application, the unique features in the medium and source-receiver configuration require special attention for the FEM grid generation. First, the borehole is elliptical in general (the circular one being a special case), and both the source and receiver are located in the borehole. Second, the medium far away from the borehole has a small effect on the field since the field is generated and measured in the borehole. These features call for an expanding grid as shown in Fig. 4(a) (only a quarter is shown). To reduce the bandwidth of the matrices, we use a rebookkeeping procedure: the indexing starts with the left-most node on the outer circle, and slides along vertical direction to the right. This reduces the bandwidth to the number of nodes on the diameter line. Alternatively, a more efficient approach is to transform the rectangular grid into an elliptical grid. The minimum bandwidth of the modified rectangular grid remains unchanged. Fig. 4(b) shows the central part of the modified rectangular grid (unoptimized).

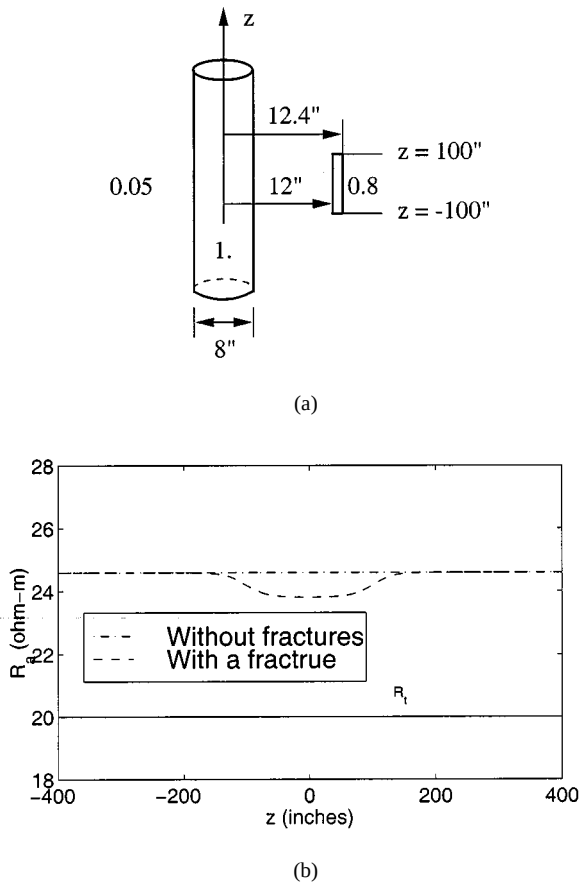

Fig. 6. Vertical fracture. (a) Geometry. (b) Apparent resistivity distribution.

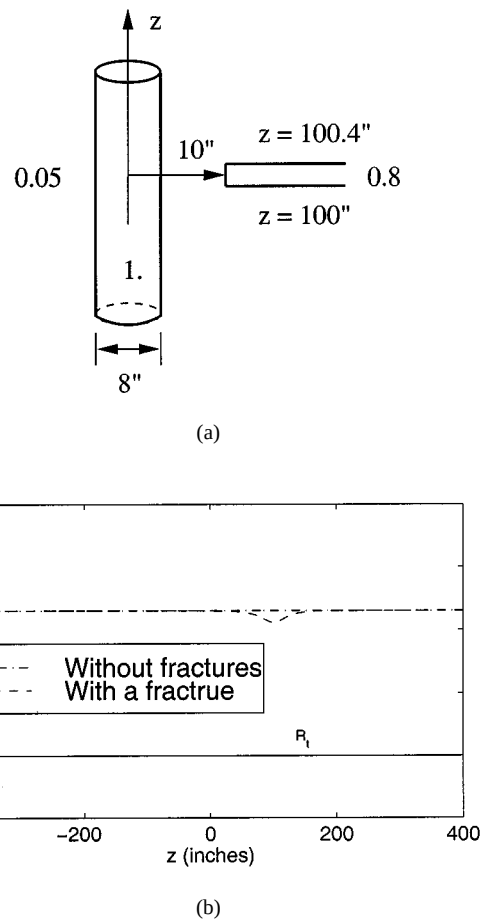

Fig. 7. Horizontal fracture. (a) Geometry. (b) Apparent resistivity distribution.

Conventionally, in vertical wells the invasion zone around the borehole is assume circular. However, for deviated wells, the invasion zone can have a different shape because of nonsymmetric mud filtration into the formation. Since the NMM method uses a 2-D FEM, it can model inhomogeneous invasion zones of arbitrary shape. Fig. 5(a) shows a four-layer medium with elliptical invaded zones in the center layers. In this and the following figures, R_t refers to the formation resistivity (i.e., the outer zone), and R_{x0} refers to the resistivity of the invaded zone (i.e., the zone between the borehole and the outer zone). The long and short half axes for the two ellipses are (20, 12) in and (12, 10) in, respectively. For comparison, both the results for the elliptical invasion and circular invasion with radii the same as the short axes of the elliptical invasion are shown in Fig. 5(b). The difference between two results is displayed. In addition, the effects of borehole are also shown clearly outside the inhomogeneous region. Because of the generality of the 2-D FEM for the eigenvalue problems, the 3-D NMM method can model inhomogeneous invasion zones of arbitrary shape.

Fractures are often encountered in well logging. Here, we consider vertical and horizontal fractures. In these examples, the fracture conductivity is $\sigma = 0.8$ S/m. Fig. 6(a) shows a vertical fracture in a formation, with the cross section of 0.4 in $\times$ 200 in. Fig. 7(a) shows a half-plane horizontal fracture. Fig. 6(b) and 7(b) display the apparent resistivity for the formation with vertical and horizontal fractures, respectively. For comparison, we also show the results without fractures. It can be seen that the fractures have notable effects on the measurement even though their thickness is very small.

Horizontal wells are becoming increasingly popular because of the potentially significant increase in the yield. Fig. 8(a) shows a horizontal well in a three-layer medium, with an invasion zone in the center layer. The medium has three vertical regions and is symmetric about $z = 0$ plane (z-axis is chosen along the axis of borehole). Fig. 8(b) shows the result for the apparent resistivity measured in the formation.

IV. Conclusion

A full 3-D numerical mode-matching (NMM) technique is developed for modeling the distribution of electric potentials in 3-D conductive media in resistivity well logging. The fields due to an arbitrary electric current source can be obtained with the help of Green's function. The accuracy of the 3-D NMM method is verified for several 3-D inhomogeneous media. We demonstrate some typical applications of the 3-D NMM algorithm in resistivity well logging, including invasion zones of noncircular shape, vertical and horizontal fractures, and horizontal wells. The proposed algorithm is directly applicable to wave propagation in 3-D stratified media.

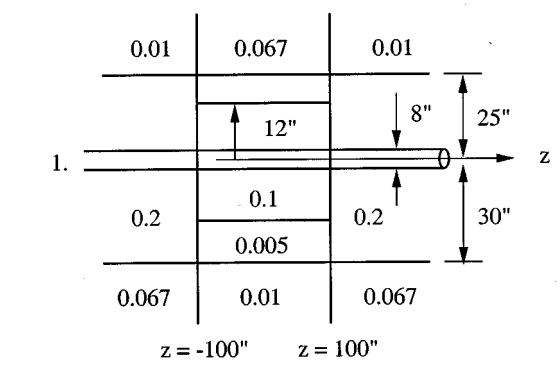

(a)

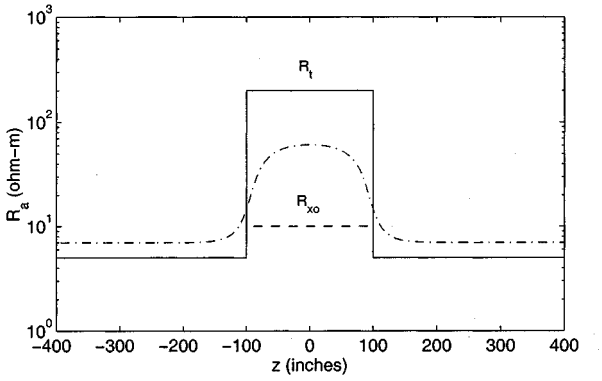

(b)

Fig. 8. Horizontal well. (a) Geometry. (b) Apparent resistivity distribution.

APPENDIX
MODE-MATCHING (MM) SOLUTION FOR A THREE-LAYER COAXIAL CYLINDER

Consider the electric potential in a three-layer coaxial cylinder of the inner radius a_1 and outer radius a_2, with constant conductivities σ_1 and σ_2 in the inner and outer cylinders, respectively. On the surface $\rho = a_2$, the electric potential is zero.

Let

$$u_1 = \sum_{m=0}^{\infty} A_m J_m(k_{mz}\rho)\cos m(\phi-\phi')Z(k_{mz}z) \qquad \rho < a_1 \tag{A.1}$$

$$u_2 = \sum_{m=0}^{\infty} B_m Z_m(k_{mz}\rho)\cos\, m(\phi-\phi')Z(k_{mz}z) \qquad \rho > a_1 \tag{A.2}$$

where

$$Z_m(k_{mz}\rho) = J_m(k_{mz}\rho)Y_m(k_{mz}a_2) - Y_m(k_{mz}\rho)J_m(k_{mz}a_2). \tag{A.3}$$

Applying the boundary conditions at $\rho = a_1$

$$u_1 = u_2, \qquad \sigma_1 \frac{\partial u_1}{\partial \rho} = \sigma_2 \frac{\partial u_2}{\partial \rho} \tag{A.4}$$

to (A.1) and (A.2), we get the following eigenvalue equation:

$$\sigma_1 J_m'(k_{mz}a_1)Z_m(k_{mz}a_1) - \sigma_2 J_m(k_{mz}a_1)Z_m'(k_{mz}a_1) = 0. \tag{A.5}$$

The roots of the above equation are the eigenvalues k_{mz}, denoted as k_{mn} $(n = 1, 2, \cdots)$. The corresponding eigenmodes are given by

$$\Phi_{mn}(\boldsymbol{\rho}) = R_{mn}(\rho)\cos m(\phi-\phi') \tag{A.6}$$

where the radial functions are defined as

$$R_{mn}(\rho) = \begin{cases} A_{mn}J_m(k_{mn}\rho) & \rho < a_1 \\ B_{mn}Z_m(k_{mn}\rho) & \rho > a_1 \end{cases} \tag{A.7}$$

with $A_{mn} = Z_m(k_{mn}a_1)/J_m(k_{mn}a_1)$ and $B_{mn} = 1$.

The eigenmodes in (A.6) can be normalized by using the following normalization constants:

$$\begin{aligned} N_{mn} &= \langle \Phi_{mn}, \sigma\Phi_{mn}\rangle \\ &= \int_0^{2\pi i}\int_0^{a_2} \Phi_{mn}(\boldsymbol{\rho})\sigma(\boldsymbol{\rho})\Phi_{mn}(\boldsymbol{\rho})\rho\, d\rho\, d\phi \\ &= 2\pi(\delta_{0m}+1)\Big\{\sigma_1 A_m^2 \int_0^{a_1} J_m^2(k_{zn}\rho)\rho\, d\rho \\ &\qquad + \sigma_2 B_m^2 \int_{a_1}^{a_2} Z_m^2(k_{zn}\rho)\rho\, d\rho\Big\}. \end{aligned} \tag{A.8}$$

It can be shown that the above eigenmodes are orthogonal with the inner product defined in (3).

The mode conversion matrix elements between lth and $(l+1)$th layers are given by

$$\begin{aligned} &Q_{l,\,l+1}^{mn,\,m'n'} \\ &= \left\langle \Phi_{mn}^{(l)}, \sigma^{(l)}\Phi_{m'n'}^{(l+1)}\right\rangle \\ &= (1+\delta_{0m})\pi\delta_{mm'}\int_0^{a_2} \sigma^{(l)} R_{mn}^{(l)}(\rho)R_{m'n'}^{(l+1)}(\rho)\rho\, d\rho \\ &= (1+\delta_{0m})\pi\delta_{mm'} \\ &\quad \cdot\Big[\sigma_1^{(l)}A_{mn}^{(l)}A_{m'n'}^{(l+1)}\int_0^{a_1} J_m(k_{mn}^{(l)}\rho)J_m(k_{mn'}^{(l+1)}\rho)\rho\, d\rho \\ &\qquad + \sigma_2^{(l)}B_{mn}^{(l)}B_{m'n'}^{(l+1)}\int_{a_1}^{a_2} Z_m(k_{mn}^{(l)}\rho)Z_m(k_{mn'}^{(l+1)}\rho)\rho\, d\rho\Big] \end{aligned} \tag{A.9}$$

where the superscript (l) denotes quantities associated with lth layer. The local reflection and transmission matrices then have the same formulas as (13) and (14).

The integrals in (A.8) and (A.9) can be analytically carried out by using the following formulas [25]:

$$\int^z zZ_\nu^2(kz)\, dz = \frac{1}{2}z^2\left[Z_\nu'^2(kz) + \left(1-\frac{\nu^2}{k^2z^2}\right)Z_\nu^2(kz)\right] \tag{A.10}$$

and

$$\int^{z} zZ_\nu(kz)Z_\nu(lz)\,dz = \frac{z}{k^2-l^2}\left[lZ_\nu(kz)Z'_\nu(lz) - kZ_\nu(lz)Z'_\nu(kz)\right] \qquad k \neq l \tag{A.11}$$

where $Z_\nu(kz)$ can be a Bessel's functions or a cross product of Bessel's functions.

The Green's functions for a single layer can then be expanded in terms of the above eigenmodes as

$$G(\mathbf{r}, \mathbf{r}') = \sum_{m=0}^{\infty}\sum_{n=1}^{\infty}\frac{1}{2k_{mn}}R_{mn}(\rho)R_{mn}(\rho') \cdot \cos m(\phi-\phi')e^{-k_{mn}|z-z'|}. \tag{A.12}$$

This has the same vector form as (8) with the same definition of parameters.

Now we construct the Green's function for a three-layer coaxial cylinder. When the source is located in 1st layer, we have

$$G_1(\mathbf{r}, \mathbf{r}') = \mathbf{\Phi}_1^t(\boldsymbol{\rho})\cdot\left[e^{-\overline{\mathbf{K}}_{1z}|z-z'|} + e^{-\overline{\mathbf{K}}_{1z}(z_1-z)} \cdot\tilde{\overline{\mathbf{R}}}_{12}\cdot e^{-\overline{\mathbf{K}}_{1z}(z_1-z')}\right]\cdot\mathbf{S}_1(\boldsymbol{\rho}') \tag{A.13}$$

$$G_2(\mathbf{r}, \mathbf{r}') = \mathbf{\Phi}_2^t(\boldsymbol{\rho})\cdot\left[e^{-\overline{\mathbf{K}}_{2z}(z-z_1)} + e^{-\overline{\mathbf{K}}_{2z}(z_2-z)} \cdot\overline{\mathbf{R}}_{23}\cdot\overline{\mathbf{P}}_{12}\right]\cdot\mathbf{A}_2 \tag{A.14}$$

$$G_3(\mathbf{r}, \mathbf{r}') = \mathbf{\Phi}_3^t(\boldsymbol{\rho})\cdot e^{-\overline{\mathbf{K}}_{3z}(z-z_2)}\cdot\mathbf{A}_3. \tag{A.15}$$

Applying the constraint conditions [16] at the interfaces $z = z_1$ and $z = z_2$, the unknowns $\mathbf{A}_2$ and $\mathbf{A}_3$ can be found as

$$\mathbf{A}_2 = \overline{\mathbf{M}}_2^{(+)}\cdot\overline{\mathbf{T}}_{12}\cdot e^{-\overline{\mathbf{K}}_{1z}(z_1-z')}\cdot\mathbf{S}_1(\boldsymbol{\rho}') \tag{A.16}$$

$$\mathbf{A}_3 = \overline{\mathbf{T}}_{23}\cdot\overline{\mathbf{P}}_{12}\cdot\mathbf{A}_2 \tag{A.17}$$

and other matrices such as $\tilde{\overline{\mathbf{R}}}_{12}$ and $\overline{\mathbf{M}}_2^{(+)}$, have the same definition as in Section II.

When the source is located in second layer, we write

$$G_1(\mathbf{r}, \mathbf{r}') = \mathbf{\Phi}_1^t(\boldsymbol{\rho})\cdot e^{-\overline{\mathbf{K}}_{1z}(z_1-z)}\cdot\mathbf{B} \tag{A.18}$$

$$G_2(\mathbf{r}, \mathbf{r}') = \mathbf{\Phi}_2^t(\boldsymbol{\rho})\cdot\left[e^{-\overline{\mathbf{K}}_{2z}|z-z'|}\cdot\mathbf{S}_2(\boldsymbol{\rho}') + e^{-\overline{\mathbf{K}}_{2z}(z-z_1)}\cdot\mathbf{C} + e^{-\overline{\mathbf{K}}_{2z}(z_2-z)}\cdot\mathbf{D}\right] \tag{A.19}$$

$$G_3(\mathbf{r}, \mathbf{r}') = \mathbf{\Phi}_3^t(\boldsymbol{\rho})\cdot e^{-\overline{\mathbf{K}}_{3z}(z-z_2)}\cdot\mathbf{A}. \tag{A.20}$$

Using the boundary conditions at $z = z_1$ and $z = z_2$, introducing the appropriate inner products, and by means of the orthogonality of eigenmodes, we can determine the four unknown vectors $\mathbf{A}$, $\mathbf{B}$, $\mathbf{C}$ and $\mathbf{D}$. The reduced matrix equations are

$$\overline{\boldsymbol{\alpha}}_{11}\cdot\mathbf{C} + \overline{\boldsymbol{\alpha}}_{12}\cdot\mathbf{D} = \mathbf{b}_1 \tag{A.21}$$

$$\overline{\boldsymbol{\alpha}}_{21}\cdot\mathbf{C} + \overline{\boldsymbol{\alpha}}_{22}\cdot\mathbf{D} = \mathbf{b}_2 \tag{A.22}$$

where

$$\overline{\boldsymbol{\alpha}}_{11} = \overline{\mathbf{K}}_{1z}\cdot\overline{\mathbf{Q}}_{12} + \overline{\mathbf{Q}}_{21}^t\cdot\overline{\mathbf{K}}_{2z} \tag{A.23}$$

$$\overline{\boldsymbol{\alpha}}_{12} = \left(\overline{\mathbf{K}}_{1z}\cdot\overline{\mathbf{Q}}_{12} - \overline{\mathbf{Q}}_{21}^t\cdot\overline{\mathbf{K}}_{2z}\right)\cdot\overline{\mathbf{P}}_{12} \tag{A.24}$$

$$\overline{\boldsymbol{\alpha}}_{21} = \left(\overline{\mathbf{K}}_{2z}\cdot\overline{\mathbf{Q}}_{23} - \overline{\mathbf{Q}}_{32}^t\cdot\overline{\mathbf{K}}_{3z}\right)^t\cdot\overline{\mathbf{P}}_{12} \tag{A.25}$$

$$\overline{\boldsymbol{\alpha}}_{22} = -\left(\overline{\mathbf{K}}_{2z}\cdot\overline{\mathbf{Q}}_{23} + \overline{\mathbf{Q}}_{32}^t\cdot\overline{\mathbf{K}}_{3z}\right)^t \tag{A.26}$$

and

$$\mathbf{b}_1 = -\left(\overline{\mathbf{K}}_{1z}\cdot\overline{\mathbf{Q}}_{12} - \overline{\mathbf{Q}}_{21}^t\cdot\overline{\mathbf{K}}_{2z}\right)\cdot e^{-\overline{\mathbf{K}}_{2z}(z'-z_1)}\cdot\mathbf{S}_2(\boldsymbol{\rho}') \tag{A.27}$$

$$\mathbf{b}_2 = -\left(\overline{\mathbf{K}}_{2z}\cdot\overline{\mathbf{Q}}_{23} - \overline{\mathbf{Q}}_{32}^t\cdot\overline{\mathbf{K}}_{3z}\right)\cdot e^{-\overline{\mathbf{K}}_{2z}(z_2-z')}\cdot\mathbf{S}_2(\boldsymbol{\rho}'). \tag{A.28}$$

We can solve (A.21) and (A.22) for $\mathbf{C}$ and $\mathbf{D}$ to yield

$$\mathbf{D} = \left(\overline{\boldsymbol{\alpha}}_{22} - \overline{\boldsymbol{\alpha}}_{21}\cdot\overline{\boldsymbol{\alpha}}_{11}^{-1}\cdot\overline{\boldsymbol{\alpha}}_{12}\right)^{-1}\cdot\left(\mathbf{b}_2 - \overline{\boldsymbol{\alpha}}_{21}\cdot\overline{\boldsymbol{\alpha}}_{11}^{-1}\cdot\mathbf{b}_1\right) \tag{A.29}$$

$$\mathbf{C} = \overline{\boldsymbol{\alpha}}_{11}^{-1}\cdot\left(\mathbf{b}_1 - \overline{\boldsymbol{\alpha}}_{12}\cdot\mathbf{D}\right). \tag{A.30}$$

The other two unknown vectors $\mathbf{A}$ and $\mathbf{B}$ are given by

$$\mathbf{A} = \overline{\mathbf{Q}}_{32}\cdot\left[e^{-\overline{\mathbf{K}}_{2z}(z_2-z')}\cdot\mathbf{S}_2(\boldsymbol{\rho}') + \overline{\mathbf{P}}_{12}\cdot\mathbf{C} + \mathbf{D}\right] \tag{A.31}$$

$$\mathbf{B} = \overline{\mathbf{Q}}_{12}\cdot\left[e^{-\overline{\mathbf{K}}_{2z}(z'-z_1)}\cdot\mathbf{S}_2(\boldsymbol{\rho}') + \mathbf{C} + \overline{\mathbf{P}}_{12}\cdot\mathbf{D}\right]. \tag{A.32}$$

Finally, when the source is located in third layer, the Green's function in each layer becomes

$$G_1(\mathbf{r}, \mathbf{r}') = \mathbf{\Phi}_1^t(\boldsymbol{\rho})\cdot e^{-\overline{\mathbf{K}}_{1z}(z_1-z)}\cdot\mathbf{B}_1 \tag{A.33}$$

$$G_2(\mathbf{r}, \mathbf{r}') = \mathbf{\Phi}_2^t(\boldsymbol{\rho})\cdot\left[e^{-\overline{\mathbf{K}}_{2z}(z-z_1)}\cdot\overline{\mathbf{R}}_{21}\cdot\overline{\mathbf{P}}_{12} + e^{-\overline{\mathbf{K}}_{2z}(z_2-z)}\right]\cdot\mathbf{B}_2 \tag{A.34}$$

$$G_3(\mathbf{r}, \mathbf{r}') = \mathbf{\Phi}_3^t(\boldsymbol{\rho})\cdot\left[e^{-\overline{\mathbf{K}}_{3z}|z-z'|} + e^{-\overline{\mathbf{K}}_{3z}(z-z_2)}\cdot\tilde{\overline{\mathbf{R}}}_{32}\cdot e^{-\overline{\mathbf{K}}_{3z}(z'-z_2)}\right]\cdot\mathbf{S}_3(\boldsymbol{\rho}'). \tag{A.35}$$

A similar procedure as in the case of the source in the first layer results

$$\mathbf{B}_2 = \overline{\mathbf{M}}_2^{(-)}\cdot\overline{\mathbf{T}}_{32}\cdot e^{-\overline{\mathbf{K}}_{3z}(z'-z_2)}\cdot\mathbf{S}_3(\boldsymbol{\rho}') \tag{A.36}$$

$$\mathbf{B}_1 = \overline{\mathbf{T}}_{21}\cdot\overline{\mathbf{P}}_{12}\cdot\mathbf{B}_2 \tag{A.37}$$

and other parameters also have the definition same as in Section II.

Since all integrals in the above have analytical expressions, this MM solution becomes very efficient. The above eigenmode

solutions, combined with the recursive solution of the NMM method in Section II, can be extended to model multiple horizontally and cylindrically layered media.

ACKNOWLEDGMENT

The authors thank two reviewers for their constructive suggestions to improve the manuscript.

REFERENCES

[1] H. G. Doll, "The Laterolog: a new resistivity logging method with electrodes using an automatic focusing system," *Petroleum Trans. AIME*, vol. 192, pp. 305–315, 1951.
[2] K. Kunz and J. H. Moran, "Some effects of formation anisotropy on resistivity measurements in boreholes," *Geophys.*, vol. 23, pp. 770–794, 1958.
[3] O. Koefoed, *Geosounding Principles 1—Resistivity Sounding Measurements*. New York: Elsevier, 1979.
[4] J. R. Wait, *Geo-Electromagnetism*. New York: Academic, 1982.
[5] D. Drahos, "Electrical modeling of the inhomogeneous invaded zone," *Geophys.*, vol. 49, pp. 1580–1585, Oct. 1984.
[6] S. Gianzero and B. Anderson, "An integral transform solution to the fundamental problem in resistivity logging," *Geophys.*, vol. 47, pp. 946–956, 1982.
[7] B. Anderson, T. D. Barber, J. Singer, and T. Broussard, "ELMOD—Putting electro-magnetic modeling to work to improve resistivity log interpretation," in *Proc. Trans. SPWLA 30th Annu. Logging Symp.*, New Orleans, LA, 1989, paper M.
[8] J. Li and L. C. Shen, "Numerical simulation of spherically focused logs," *Log Analyst*, vol. 33, pp. 495–499, 1992.
[9] W. C. Chew, S. Barone, B. Anderson, and C. Hennessy, "Diffraction of axisymmetric waves in a borehole by bed boundary discontinuities," *Geophys.*, vol. 49, pp. 1586–1595, Oct. 1984.
[10] L. Tsang, A. K. Chang, and S. Gianzero, "Solution of the fundamental problem in resistivity logging with a hybrid method," *Geophys.*, vol. 49, pp. 1596–1604, Oct. 1984.
[11] W. C. Chew and B. Anderson, "Propagation of electromagnetic waves though geological beds in a geophysical probing environment," *Radio Sci.*, vol. 20, pp. 611–621, 1985.
[12] W. C. Chew, "Response of a source on top of a vertically stratified half-space," *IEEE Trans. Antennas Propagat.*, vol. AP-33, pp. 649–654, June 1985.
[13] V. L. Druskin and L. A. Knizhnerman, "A method of solution of forward problems of electric well logging and electric exploration with direct current," *Izvestiya, Earth Phys.*, vol. 23, pp. 317–323, 1987.
[14] V. L. Druskin and T. V. Tamarchenko, "Fast variant of partial domain method for solution of the problem of induction logging," *Geologiya i Geofizika*, vol. 29, pp. 129–135, 1988.
[15] Q. H. Liu, B. Anderson, and W. C. Chew, "Modeling low-frequency electrode-type resistivity tools in invaded beds," *IEEE Trans. Geosci. Remote Sensing*, vol. 32, pp. 494–498, May 1994.
[16] W. C. Chew, *Waves and Fields in Inhomogeneous Media*. New York: Van Nostrand Reinhold, 1990.
[17] Q. H. Liu and W. C. Chew, "Numerical mode matching method for the multiregion vertically stratified media," *IEEE Trans. Antennas Propagat.*, vol. 38, pp. 498–506, Apr. 1990.
[18] W. C. Chew, Z. Nie, Q. H. Liu, and B. Anderson, "An efficient solution for the response of electrical well logging tools in a complex environment," *IEEE Trans. Geosci. Remote Sensing*, vol. 29, pp. 308–313, Mar. 1991.
[19] Q. H. Liu and W. C. Chew, "Diffraction of nonaxisymmetric waves in cylindrical layered media by horizontal discontinuities," *Radio Sci.*, vol. 27, pp. 569–581, 1992.
[20] Q. H. Liu, "Electromagnetic field generated by an off-axis source in a cylindrically layered medium with an arbitrary number of horizontal discontinuities," *Geophys.*, vol. 58, pp. 616–625, May 1993.
[21] ——, "Nonlinear inversion of electrode-type resistivity measurements," *IEEE Trans. Geosci. Remote Sensing*, vol. 32, pp. 499–507, May 1994.
[22] J. M. Jin, *The Finite Element Method in Electromagnetics*. New York: Wiley, 1993.
[23] A. V. Knyazev and A. L. Skorokhodov, "The preconditioned gradient-type iterative methods in a subspace for partial generalized symmetric eigenvalue problem," *SIAM J. Numer. Anal.*, vol. 31, pp. 1226–1239, 1994.
[24] G. L. G. Sleijpen, A. G. L. Booten, D. R. Fokkema, and H. A. Van der Vorst, "Jacobi–Davidson type methods for generalized eigenproblems and polynomial eigenproblems," *BIT*, vol. 36, pp. 595–633, 1996.
[25] Y. L. Luke, *Integrals of Bessel Functions*. New York: McGraw-Hill, 1962.

Guo-Xin Fan (M'97–SM'00) received the Ph.D. degree in electrical engineering from Tsinghua University, Beijing, China, in 1995.

From 1985 to 1990, he was engaged in research as a Research Engineer and the Head of a research group on the theory and techniques on subsurface detection at the China Research Institute of Radiowave Propagation, Xinxiang, China. He was in charge of the development of the first practical ground-penetrating radar in China. From September 1995 to August 1997, he was a Postdoctoral Research Fellow in the Electromagnetics Laboratory, Department of Electrical and Computer Engineering, University of Illinois at Urbana-Champaign. From August 1997 to September 1999, he was a Postdoctoral Research Associate in the Electromagnetics Laboratory, Klipsch School of Electrical and Computer Engineering, New Mexico State University, Las Cruces. Since October 1999, he has been a Research Associate in the Department of Electrical and Computer Engineering, Duke University, Durham, NC. His research interests include computational electromagnetics, electromagnetic scattering, slotted-waveguide array antenna, subsurface target detection, and development of ground-penetrating radar.

Dr. Fan was the first winner of a Science and Technology Progress Award of the Ministry of Electronics Industry of China in 1991.

Qing Huo Liu (S'88–M'89–SM'94) received the Ph.D. degree in electrical engineering from the University of Illinois at Urbana-Champaign in 1989.

From September 1986 to December 1988, he was with the Electromagnetics Laboratory, University of Illinois at Urbana-Champaign, as a Research Assistant and from January 1989 to February 1990 as a Postdoctoral Research Associate. He was a Research Scientist and Program Leader with Schlumberger-Doll Research, Ridgefield, CT, from 1990 to 1995. From October 1995 to May 1999, he was a Faculty Member at New Mexico State University, Las Cruces. Since June 1999, he has been an Associate Professor of Electrical Engineering at Duke University, Durham, NC. He has published more than 100 papers in refereed journals and conference proceedings. His research interests include computational electromagnetics and acoustics and their applications, wave propagation in inhomogeneous media, geophysical subsurface sensing, and inverse problems.

Dr. Liu is a member of Phi Kappa Phi, Tau Beta Pi, SEG, and a full member of the U.S. National Committee of URSI Commissions B and F. He currently serves as an Associate Editor for IEEE TRANSACTIONS ON GEOSCIENCE AND REMOTE SENSING. He received a Presidential Early Career Award for Scientists and Engineering (PECASE) from the National Science and Technology Council (NSTC) and an Early Career Research Award from the National Science Foundation in 1997.

Sean P. Blanchard received the B.S. degree in physics from the California Polytechnic University of Pomona, CA, in 1991 and the M.S. degrees in physics and electrical engineering from New Mexico State University, Las Cruces, in 1998 and 2000, respectively.

From 1998 to 1999, he was a Software Engineer and Systems Manager at the Idaho National Environmental and Engineering Laboratory. He is currently working on the Blue Mountain ASCI Project as a Systems Analyst for Silicon Graphics, Inc., Los Alamos National Laboratory, NM.